Journal of Materials Chemistry A

Accepted Manuscript

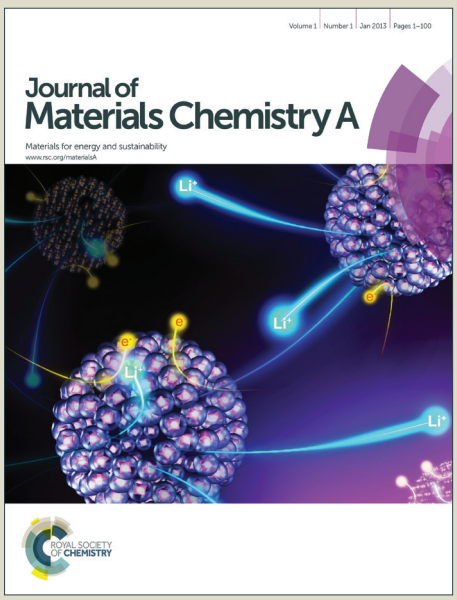

ROYAL SOCIETY OF CHEMISTRY

www.rsc.org/materialsA

Cite this: DOI: 10.1039/c0xx00000x

www.rsc.org/xxxxxx

ARTICLE TYPE

Hierarchical Structure $LiFePO_4$@C Synthesized by Oleylamine-Mediated Method for Low Temperature Applications

Jingmin Fan, Jiajia Chen, Yongxiang Chen, Haihong Huang, Zhikai Wei, Ming-sen Zheng* and Quanfeng Dong*

Received (in XXX, XXX) Xth XXXXXXXXX 20XX, Accepted Xth XXXXXXXXX 20XX
DOI: 10.1039/b000000x

In this paper, a hierarchical nanostructure $LiFePO_4$@C composite was firstly fabricated by oleylamine mediated method. The oleylamine played a multi-functional role in restricting the particle size, and forming the porous nano-structure of $LiFePO_4$@C composite. Benefiting from its hierarchical structure, $LiFePO_4$@C exhibited superior electrochemical performance, especially at low temperature. It can deliver the capacity of 117 mAh g^{-1} at current density up to 700 mA g^{-1} (about 5 C) at -20 °C.

Since Padhi's work at 1997,[1] olivine-type lithium transition-metal phosphates have attracted considerable attentions as one of the most promising lithium ion battery cathode materials for electric vehicles (EVs), plug-in hybrid electric vehicles (HEVs) and green grid, owing to its high theoretical capacity (~170 mAh g^{-1}), durability, thermal safety and low cost.[2-5] However, comparing to the high electrical conductivity of $LiCoO_2$ (10^{-3} S cm^{-1}) and $LiMn_2O_4$ (10^{-5} S cm^{-1}),[6] $LiFePO_4$ has low electrical conductivities (10^{-9} S cm^{-1})[7] and sluggish lithium ion diffusion kinetics (at least three orders of magnitude lower than $LiCoO_2$). Numerous efforts have been paid to overcome these deficiencies, such as conductive materials coating (such as: carbon,[8] polymer[9-11], poorly crystallized pyrophosphate[12]), doping[6, 13-15] and minimizing particle size.[16, 17] According to these strategies, various methods (such as solid state reaction,[12] polyol and solvothermal,[18, 19] hydrothermal,[20] ionothermal,[21] supercritical,[22] microwave-assisted,[23] electrospinning,[24] biological,[25] and spray pyrolysis[26]) have been developed to synthesize $LiFePO_4$ with different nanostructures. Nanosized particles can provide both shorter diffusion pathway and larger surface area for charge transfer, nanoporous electrode can benefit the immersion of electrolyte, and these efforts lead to the successful commercialization of $LiFePO_4$ with viable electrochemical performance. And there have been several reports on $LiFePO_4$ with ultrahigh rate performance (up to 100 C) at room temperature.[12, 27] However, it is still a challenge for $LiFePO_4$ to achieve a considerable electrochemical performance at low temperature, which retards its practice application of the electric vehicles in winter or in cold areas. To date, $LiFePO_4$ are still difficult to operate at rate >1 C, when the temperature falls below -20 °C.

Herein, a $LiFePO_4$@C hierarchical structure with superior low temperature electrochemistry performance is firstly synthesized by oleylamine-mediated strategy. The hierarchical $LiFePO_4$@C cathode exhibited the superior electrochemical performance. It can deliver the specific capacity of 149 mAh g^{-1}, 140 mAh g^{-1}, 124 mAh g^{-1} and 107 mAh g^{-1} at 5 C, 10 C, 50 C and 100 C at room temperature, respectively. Moreover, the as-prepared $LiFePO_4$@C cathode can deliver the capacity of 117 mAh g^{-1} at current density of 700 mA g^{-1}(about 5 C) when the temperature drops to -20 °C. As shown in Scheme 1, the nano-size pristine $LiFePO_4$ particles with uniformly oleylamine coating shell were produced in the first solvothermal procedure. Then, the oleylamine converts to the uniformly carbon shell during the following sinter step, forming $LiFePO_4$@C composite. The carbon shell improves the conductivity of the electrode and prevents the agglomeration of nano $LiFePO_4$. Finally, the hierarchical $LiFePO_4$@C composite was achieved from the self-assembly of the $LiFePO_4$@C nanoparticles in micrometer scale with porous structure.

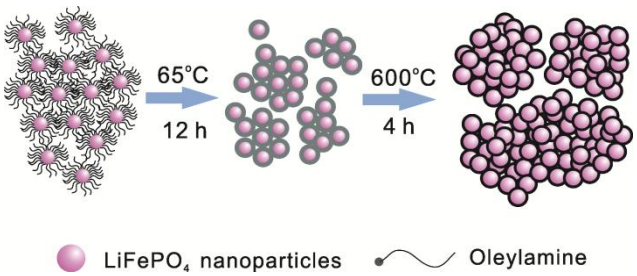

Scheme 1 The preparation process for the nano-$LiFePO_4$@C composite.

The size, morphology and crystal structure of the products were investigated by high resolution transmission electron microscopy (HRTEM), scanning electron microscopy (SEM) and X-ray diffraction (XRD). As shown in Figure 1a and 1b, $LiFePO_4$@C composite after sinter was consisted of mono-disperse primary nano particles within 30 nm, assembling into micrometer-scale particles. A thin carbon shell within 2 nm coating uniformly on the $LiFePO_4$ particles can be observed in the TEM image (Figure 1c). D and G bands of carbon occurring at 1345 cm^{-1} and 1594 cm^{-1} confirm that oleylamine can be carbonized during the sinter process and the average carbon content is determined to be 6.7 wt% by CHN element analysis (Figure S1). The porous structure and the Brunauer-Emmett-Teller (BET) surface area of $LiFePO_4$@C were also investigated

by N_2 adsorption–desorption experiments at 77 K (Figure S2). The BET surface area was measured to be 81.5 m^2 g^{-1}. The average pore diameter was as large as 6.2 nm calculated from the desorption branch of the isotherm using the Barrett–Joyner–Halenda (BJH) method, which would favor the electrolyte immersion. The high BET surface area and the narrow average pore would facilitate the diffusion of lithium ion within the hierarchical structure of $LiFePO_4$@C.[28] XRD patterns of $LiFePO_4$@C (Figure 1d) are broadened due to the nano-scale of particles and still match well with the theoretical XRD patterns of $LiFePO_4$.

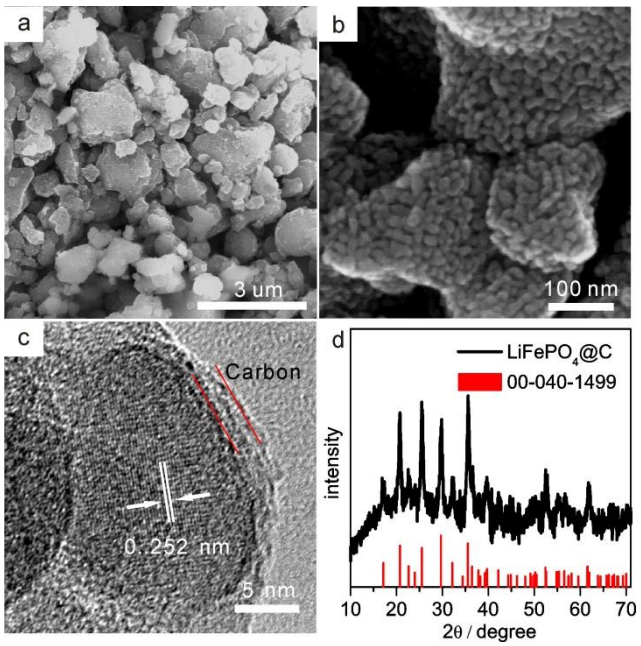

Figure 1. Morphology characterization of $LiFePO_4$@C. a, b) SEM images and c) HRTEM image of $LiFePO_4$@C composite; d) X-ray diffraction (XRD) patterns of $LiFePO_4$@C composite.

The electrochemical performance of $LiFePO_4$@C was examined by coin-type cells within 4.2-2.4 V and all the capacities were calculated based on the mass of $LiFePO_4$. The $LiFePO_4$@C cathode exhibits the superior high-rate capability (Figure 2a). It can diliver 72% capacity of its theoretical value when rate is up to 100 C without severe polarization at room temperature (Figure S3). Even under the extreme high current density (200 C rate, corresponding to 34,000 mA g^{-1}), it was also able to deliver substantial capacity of 80 mAh g^{-1}. It is among the highest value reported (Table S1).[12, 27] The as-prepared $LiFePO_4$@C cathode also exhibits excellent cycle stability. As shown in Figure 2b, no obvious fading was observed over 300 cycles at 0.5 C (85 mA g^{-1}) and 10 C (1,700 mA g^{-1}) rates. Furthermore, there was only 0.012% capacity fading per cycle when the current density was raised up to 20 C (3,400 mA g^{-1}), and with almost 100% coulombic efficiency.

At present, it is believed that the battery performance of $LiFePO_4$ drops drastically at low temperatures should be due to the sluggish lithium ion diffusion kinetic, the increasing internal resistance and electrolyte freezing.[29-31] As listed in Table S1**,** the capacity of $LiFePO_4$ was no more than 100 mAh g^{-1} at -20 °C at only 1 C rate at presnet.[27, 30-32] However, the as-prepared hierarchical nanostructure $LiFePO_4$@C demonstrated excellent electrochemical performance at low temperatures. When tested under 0 °C and -20 °C, it can deliver the capacities of 138 mAh g^{-1} and 117 mAh g^{-1} at 5 C (the current density of 700 mA g^{-1}), respectively. It should be noted that the charge current density was the same as the discharge process, and both processes were performed at the same temperature. Furthermore, no capacity fading was found during the cycling at the 5 C rate, exhibiting the excellent stability at low temperature. To our best knowledge, it is the best result of $LiFePO_4$ electrode at the -20 °C.

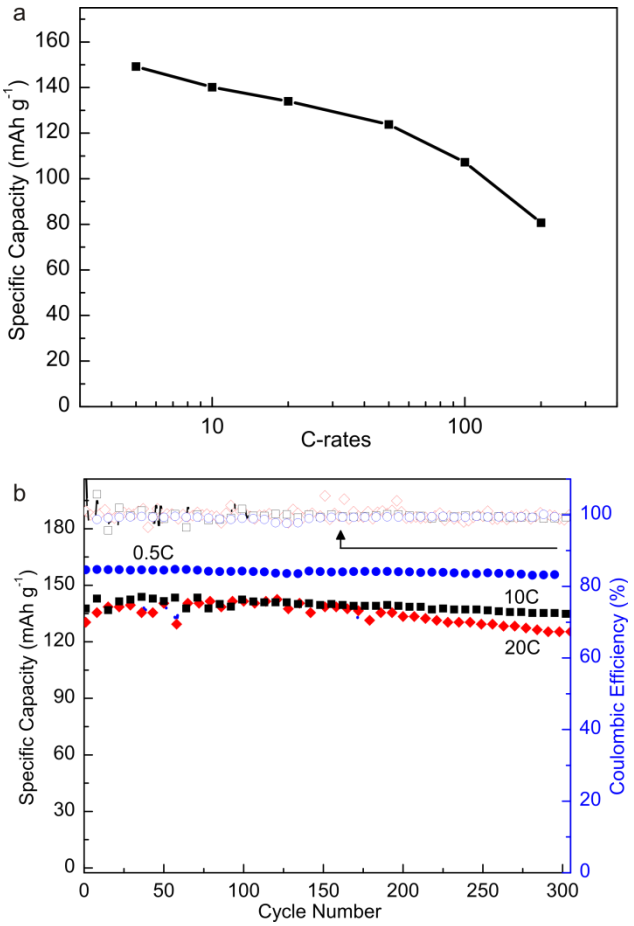

Figure 2. a) Rate performance of $LiFePO_4$@C at room temperature. b) Cycling performance of $LiFePO_4$@C. 1 C=170 mA g^{-1}.

To further understand the electrochemical kinetic of $LiFePO_4$@C composite, cyclic voltammetry (CV) and impedance measurements (EIS) were performed. ΔE_p between anodic and cathodic peaks is only 0.13 V which indicates a highly reversible redox reaction of $LiFePO_4$@C during the intercalation and deintercalation process at room temperatrue (Figure S7). Electrochemical impedance measurements of the $LiFePO_4$@C electrode at different temperatures were performed and fitted by using equivalent circuit model (Figure S8). The semicircle in the middle frequency range corresponds to the charge transfer resistance (Rct) while the sloping line in the lower frequency represents Li ion Warburg diffusion.[33] The impedance parameters derived using equivalent circuit model and diffusion coefficient are listed in Table S2.

The Rct increased from 11.73 Ω at 25 °C to 9258 Ω at -40 °C, abiding the Arrhenius equation. The Arrhenius activation energy

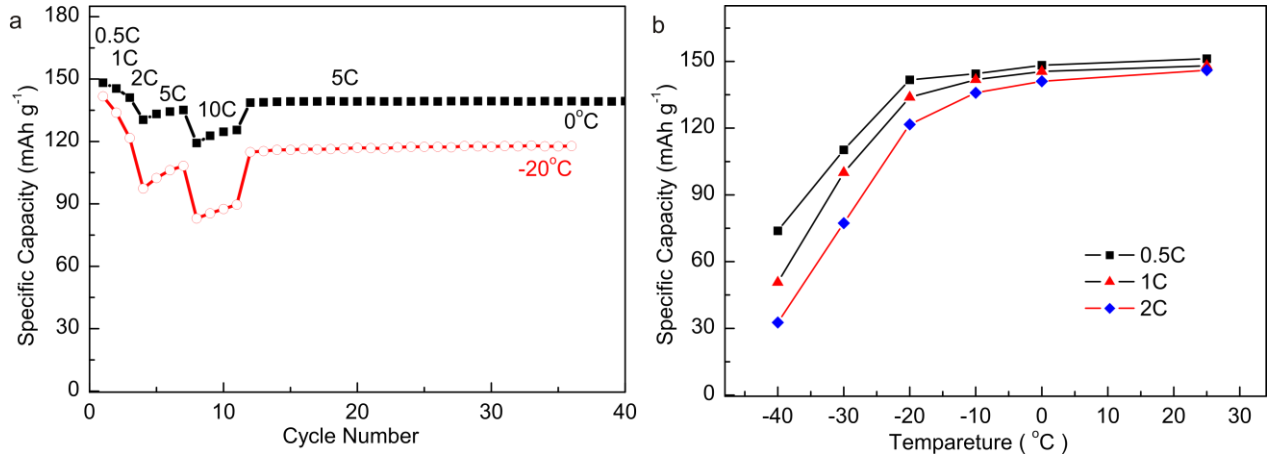

Figure 3. a) Discharge capacity versus cycle number plots of $LiFePO_4$@C from 0.5 C to 10 C and cycling at 5 C (700 mA g^{-1}) at 0 °C and -20 °C. b) Discharge capacity at 0.5 C, 1 C and 2 C on temperature in the range of -40 °C～25 °C.

is calculated to be 59.35 kJ mol^{-1} (Figure S9). High activation energy means that the charge transfer process is influenced greatly by temperatures. The linear relationship between 1000/T and ln(1/Rct) indicates that the electrode/electrolyte interface can maintain well even at -40 °C. The diffusion coefficients at various temperatures according to Warburg diffusion area of EIS results, are estimated to 3.93×10^{-12} cm^2 s^{-1} at 25 °C and is 9.23×10^{-15} cm^2 s^{-1} at -20 °C, respectively. And the diffusion time for Li^+ diffuse over 30 nm (the particle size of as-prepared $LiFePO_4$) can be estimated to be ~10 s and ~1000 s at 25 °C and -20 °C respectively, according to equation $t=L^2/D_{Li+}$ (L is the particle size). These were consistent with the electrochemical results (200C at 25 °C, around 9 s and 2 C at -20 °C, around 1300 s). The diffusion coefficients demonstrate that the limiting step of as-prepared $LiFePO_4$@C at high rate is the Li^+ diffusion kinetic in bulk phase rather than interface. When the temperature is higher than -20 °C, $LiFePO_4$@C still has the ability to retain considerable battery performance (Figure 3a and 3b). As the temperature below -20 °C, the capacities of as-prepared $LiFePO_4$@C electrode were steeply decreased from 121 mAh g^{-1} at -20 °C to 32 mAh g^{-1} at -40 °C at the current density of 2 C. The D_{Li+} no longer meets Arrhenius equation when the temperature below -20 °C (Figure S11), suggesting a more restricted electrochemical kinetics occurred. It might result from the low lithium ion diffusion coefficient in electrolyte.[34]

In summary, the superior kinetic character of as-prepared $LiFePO_4$@C electrode is benefiting from its special structure: (1) the hierarchical nano-structure constituted by particles and pores in different nano-scale; (2) every particle in the hierarchical structure is in nano-scale within 30 nm; (3) every particle in the hierarchical stucture is uniformly coated with a 2 nm carbon shell. In favor of its porous structure, uniformly carbon coating and nanosized particle, the as-prepared $LiFePO_4$@C electrode shows superior electrochemical performance, especially at low temperature, which is an important character for the practice application of EVs/HEVs in the winter. Moreover, this method can be easily extended to synthesize other energy storage materials such as $LiMnPO_4$.

Acknowledgment

The authors gratefully acknowledge the financial support from the Key Project of NSFC (U1305246, 21321062), the Major Project funded by Xiamen city (3502Z20121002).

Notes and references

Department of Chemistry, College of Chemistry and Chemical Engineering, Xiamen University, State Key Laboratory of Physical Chemistry of Solid Surfaces, Xiamen, Fujian, 361005, P. R. China.
Tel: 0592-2185905; FAX: 0592-2183905; E-mail: qfdong@xmu.edu.cn and mszheng@xmu.edu.cn

† Electronic Supplementary Information (ESI) available: Experimental details, material characterization, Electrochemical Measurements, Raman spectrum, additional electrochemical data and charge/discharge curve. See DOI: 10.1039/b000000x/

1. A. K. Padhi, K. S. Nanjundaswamy and J. B. Goodenough, *J. Electrochem. Soc.*, 1997, **144**, 1188-1194.
2. M. Armand and J. M. Tarascon, *Nature*, 2008, **451**, 652-657.
3. B. Dunn, H. Kamath and J. M. Tarascon, *Science*, 2011, **334**, 928-935.
4. Z. Yang, J. Zhang, M. C. W. Kintner-Meyer, X. Lu, D. Choi, J. P. Lemmon and J. Liu, *Chem .Rev.*, 2011, **111**, 3577-3613.
5. L.-X. Yuan, Z.-H. Wang, W.-X. Zhang, X.-L. Hu, J.-T. Chen, Y.-H. Huang and J. B. Goodenough, *Energy Environ. Sci.*, 2011, **4**, 269-284.
6. S.-Y. Chung, J. T. Bloking and Y.-M. Chiang, *Nat. Mater.*, 2002, **1**, 123-128.
7. D. W. Choi, D. H. Wang, I. T. Bae, J. Xiao, Z. M. Nie, W. Wang, V. V. Viswanathan, Y. J. Lee, J. G. Zhang, G. L. Graff, Z. G. Yang and J. Liu, *Nano Lett.*, 2010, **10**, 2799-2805.
8. J. Wang and X. Sun, *Energ. Environ. Sci.*, 2012, **5**, 5163-5185.
9. K. S. Park, S. B. Schougaard and J. B. Goodenough, *Adv. Mater.*, 2007, **19**, 848-851.
10. Y. H. Huang and J. B. Goodenough, *Chem. Mater.*, 2008, **20**, 7237-7241.
11. D. Lepage, C. Michot, G. X. Liang, M. Gauthier and S. B. Schougaard, *Angew. Chem. Int. Edit.*, 2011, **50**, 6884-6887.
12. B. Kang and G. Ceder, *Nature*, 2009, **458**, 190-193.
13. N. Meethong, Y.-H. Kao, S. A. Speakman and Y.-M. Chiang, *Adv Funct Mater*, 2009, **19**, 1060-1070.

14. C. A. J. Fisher, V. M. H. Prieto and M. S. Islam, *Chem. Mater.*, 2008, **20**, 5907-5915.
15. F. Omenya, N. A. Chernova, S. Upreti, P. Y. Zavalij, K.-W. Nam, X.-Q. Yang and M. S. Whittingham, *Chem. Mater.*, 2011, **23**, 4733-4740.
16. C. Delacourt, P. Poizot, S. Levasseur and C. Masquelier, *Electrochem. Solid-State Lett.*, 2006, **9**, A352-A355.
17. R. Malik, D. Burch, M. Bazant and G. Ceder, *Nano Lett.*, 2010, **10**, 4123-4127.
18. T. Azib, S. Ammar, S. Nowak, S. Lau-Truing, H. Groult, K. Zaghib, A. Mauger and C. M. Julien, *J. Power Sources*, 2012, **217**, 220-228.
19. D. Rangappa, K. Sone, T. Kudo and I. Honma, *J. Power Sources*, 2010, **195**, 6167-6171.
20. B. Ellis, W. H. Kan, W. R. M. Makahnouk and L. F. Nazar, *J. Mater. Chem.*, 2007, **17**, 3248-3254.
21. N. Recham, L. Dupont, M. Courty, K. Djellab, D. Larcher, M. Armand and J. M. Tarascon, *Chem. Mater.*, 2009, **21**, 1096-1107.
22. D. Rangappa, K. Sone, M. Ichihara, T. Kudo and I. Honma, *Chem. Commun.*, 2010, **46**, 7548-7550.
23. I. Bilecka, A. Hintennach, I. Djerdj, P. Novak and M. Niederberger, *J. Mater. Chem.*, 2009, **19**, 5125-5128.
24. C. B. Zhu, Y. Yu, L. Gu, K. Weichert and J. Maier, *Angew. Chem. Int. Edit.*, 2011, **50**, 6278-6282.
25. Y. J. Lee, H. Yi, W. J. Kim, K. Kang, D. S. Yun, M. S. Strano, G. Ceder and A. M. Belcher, *Science*, 2009, **324**, 1051-1055.
26. J. Liu, T. E. Conry, X. Song, M. M. Doeff and T. J. Richardson, *Energ. Environ. Sci.*, 2011, **4**, 885-888.
27. X.-L. Wu, Y.-G. Guo, J. Su, J.-W. Xiong, Y.-L. Zhang and L.-J. Wan, *Adv. Energy Mater.*, 2013, **3**, 1155-1160.
28. C. Kuss, D. Lepage, G. Liang and S. B. Schougaard, *Chemical Science*, 2013, **4**, 4223-4227.
29. X. H. Rui, Y. Jin, X. Y. Feng, L. C. Zhang and C. H. Chen, *J. Power Sources*, 2011, **196**, 2109-2114.
30. X.-Z. Liao, Z.-F. Ma, Q. Gong, Y.-S. He, L. Pei and L.-J. Zeng, *Electrochem. Commun.*, 2008, **10**, 691-694.
31. S. S. Zhang, K. Xu and T. R. Jow, *J. Power Sources*, 2006, **159**, 702-707.
32. S. W. Oh, S.-T. Myung, S.-M. Oh, K. H. Oh, K. Amine, B. Scrosati and Y.-K. Sun, *Adv. Mater.*, 2010, **22**, 4842-4845.
33. T. Muraliganth, A. V. Murugan and A. Manthiram, *J. Mater. Chem.*, 2008, **18**.
34. E. J. Plichta and W. K. Behl, *J. Power Sources*, 2000, **88**, 192-196.